J Mater Sci: Mater Med (2011) 22:1891–1900
DOI 10.1007/s10856-011-4357-9

Improved interaction of osteoblast-like cells with apatite–nanodiamond coatings depends on fibronectin

K. Hristova · E. Pecheva · L. Pramatarova · G. Altankov

Received: 23 December 2010 / Accepted: 23 May 2011 / Published online: 25 June 2011

Abstract New apatite (AP)/nanodiamond (ND) coating has been developed to improve physical and biological properties of stainless steel (SS) versus single AP coating. Homogeneously electrodeposited AP–ND layer demonstrates increased mechanical strength, interlayer cohesion and ductility. In the absence of serum, osteoblast-like MG63 cells attach well but poorly spread on both AP and AP–ND substrata. Pre-adsorption with serum or fibronectin (FN) improves the cellular interaction—an effect that is better pronounced on the AP–ND coating. In single protein adsorption study fluorescein isothiocyanate-labeled FN (FITC-FN) shows enhanced deposition on the AP–ND layer consistent with the significantly improved cell adhesion, spreading and focal adhesions formation (in comparison to SS and AP), particularly at low FN adsorption concentrations (1 μg/ml). Higher FN concentrations (20 μg/ml) abolish this difference suggesting that the promoted cellular interaction of serum (where FN is low) is caused by the greater affinity for FN. Moreover, it is found that MG63 cells tend to rearrange both adsorbed and secreted FN on the AP–ND layer suggesting facilitated FN matrix formation.

K. Hristova · G. Altankov
Institute of Biophysics and Biomedical Engineering, Bulgarian Academy of Sciences, Sofia, Bulgaria

E. Pecheva · L. Pramatarova
Laboratory of Biocompatible Materials, Institute of Solid State Physics, Bulgarian Academy of Sciences, Sofia, Bulgaria

G. Altankov (✉)
Institucio Catalana de Recercia i Estudias Avançats (ICREA), Barcelona, Spain
e-mail: george.altankov@icrea.es

K. Hristova · G. Altankov
Institute for Bioengineering of Catalonia (IBEC), Barcelona, Spain

1 Introduction

Biomimetic hydroxyapatite (HA) is highly biocompatible inorganic material from the apatite (AP) family which osseointegrates well due to its chemical resemblance to mammalian bone and teeth [1–3]. On the other hand, HA is known to be capable of adsorbing many proteins and to interact well with osteoblast precursor cells, therefore it is frequently used as a coating for metal implants because it is shown to promote faster bone adaptation, reduced healing time and enhanced bone apposition [4, 5]. However, the benefits of HA coatings are constrained by the low strength of adhesion to the implant surface and by the limited cohesion within the layer [6, 7]. It was suggested that the addition of a second minor phase could favor the mechanical and biological properties of such coatings [6, 7]. Therefore, a novel AP–ND coating has been developed to improve the biocompatibility of SS or other materials considered for osseoimplantation. This paper describes some details of its biological performance.

The successful interaction of foreign materials with cells depends on the proper adsorption of adhesive proteins from the surrounding medium, which is rapidly followed by cell adhesion and spreading [8]. Among these proteins it seems that FN and vitronectin play critical role as they exist in soluble form in most biological fluids [9]. FN is typically found in the extracellular matrix (ECM) fibrils which are involved in several fundamental biological functions including cell adhesion, migration, growth and differentiation [10–12], as well as ECM organization [13–15]. FN is one of the earliest proteins laid down during bone matrix

formation [16] and its accumulation in the areas of skeletogenesis suggests involvement in the early stages of bone formation [13, 14]; it plays a critical role in osteoblasts differentiation and survival [15]. Several studies have shown that FN is required for the assembly of multiple ECM proteins, including collagen [17], fibrinogen [18] and trombospondin [19], and for the recruitment of growth factors [20]. Conversely, plasma FN supports the initial cellular interaction with biomaterials [16, 21]. Cell adhesion to FN depends on the interaction with integrins [22]—a family of transmembrane glycoproteins consisting of α and β subunits. FN is recognized by at least 8 integrin heterodimers [23] but the main FN receptor is $\alpha_5\beta_1$ [24]. Upon binding to the ligand, integrins clusterize in focal adhesion complexes and together with other adhesive and signaling molecules form a critical linkage with the cytoskeleton [22, 25, 26]. Therefore, the proper development of focal adhesion complexes may characterize the effectiveness of cell–material interaction.

The electrodeposited AP–ND layer demonstrated increased mechanical strength, interlayer cohesion and ductility. For a comprehensive characterization of biocompatibility, AP–ND coatings were seeded with osteoblast-like MG63 cells and their interaction was compared with plain SS and single AP coating under short term culture conditions. Osteoblasts are the principal cells in the bone matrix and their successful interaction with given material provides insight to its osseointegration [27]. We studied cell adhesion to plain SS, AP and AP–ND surfaces, as well as after serum or FN pre-adsorption following the overall cell morphology and the organization of focal adhesion complexes, further quantifying cell adhesion and spreading. A pronounced effect of FN was observed and the results were corroborated with the observed increased quantities of FITC-FN adsorption and the allowance of adhering cells to better organize FN matrix on the AP–ND coating.

2 Materials and methods

2.1 Samples preparation

Coatings were prepared by cathodic electrodeposition (ED) on mirror-polished austenitic SS substrates (AISI 316L) from simulated body fluid (SBF). The SBF electrolyte resembled the ion composition, concentrations and pH of the human blood plasma. It was prepared by dissolving the reagent grade chemicals NaCl, $NaHCO_3$, KCl, $K_2HPO_4{\cdot}3H_2O$, $MgCl_2{\cdot}6H_2O$, $Na_2SO_4{\cdot}10H_2O$, and $CaCl_2{\cdot}2H_2O$ in distilled water and buffering at pH 7.4 with *tris*-hydroxymethyl-aminomethane and hydrochloric acid [28, 29].

ND particles (4–6 nm, density 3.2 g/cm^3, content of diamond 97–99%) were synthesized by shock-wave propagation method through the detonation of explosives at high pressure and high temperature produced in the detonation. Subsequent purification from graphite by applying oxidation with potassium dichromate in sulphuric acid was carried out, and after several washings with hydrochloric acid and water, the as-obtained ND powder was dried [30]. The purification method generally leads to an oxidation of the ND surface, which was covered by carboxyl, and to a lesser extent by carbonyl and hydroxyl groups [30]. The nanometer-sized ND particles were added to the SBF electrolyte in a concentration of 0.5 g/l and ultrasonically shaken for 15 min before the ED. A potentiostat (Hokuto Denko HA150G) was used for the ED, which was performed at 37°C by sweeping the potential from the open circuit potential of SS (-0.180 V_{SCE} in ND-SBF) to -1.5 V_{SCE} at a rate of 10 mV/s and maintaining this value for 1 h. After the deposition, the coated samples were washed under a flow of distilled water and dried in air. Two groups of samples were thus prepared: (i) by ED for 1 h from ND-containing SBF (samples named AP–ND) and (ii) by ED for 1 h from pure SBF (samples named AP and used as controls of the first group). Mirror-polished SS substrates were also used as controls. For further biological studies, the three groups of samples were sterilized via autoclaving.

The morphology and elemental composition of AP–ND and AP coatings were studied by scanning electron microscopy (SEM; Hitachi S-3400 NX, 12 kV) coupled with energy dispersive X-ray spectroscopy (EDX; performed over five areas with size of 20 $\times$ 25 μm, as well as from five points taken on white aggregates) for calculation of the Ca:P ratio. The coatings structure was examined by Fourier transform infrared spectroscopy (FTIR; Bomem IR spectrometer FTLA2000, ABB Inc., 100 scans, resolution of 4 cm^{-1}) in reflection mode. Coatings thickness, peel and shear strengths were measured by surface and interfacial cutting analysis system (SAICAS CN-20R; cutting blade diamond width of 0.3 mm) at a constant load mode set to $F_{vertical} = F_{horizontal} = 0.01$ N. Five measurements were carried out for each group to estimate the peel and shear strengths. Vickers hardness (HV) was estimated by a HMV-1 micro hardness tester (Shimadzu) with a load of 245 mN applied normally to the coatings for 10 s. Other loads (98, 490 or 980 mN) were also applied for comparison. Average hardness values were calculated from five indents made for each sample.

2.2 Preparation of FITC-labeled FN

Human plasma FN (Sigma, F2006) was dissolved in 0.1 M sodium bicarbonate buffer (pH 9.0) at 1 mg/ml, then 10 μl

of FITC (Sigma, F7378) in dimethyl sulfoxide from a stock of 10 mg/ml was added. The mixture was incubated for 2 h at 37°C. The labeled FN was separated from unreacted dye on a Sephadex G-25 equilibrated with phosphate buffered saline (PBS) solution. The final protein concentration was estimated by measuring the absorbance at 280 nm, while the degree of FITC-labeling was calculated against the absorbance at 494 nm. The aliquots were then stored at −20°C.

To obtain qualitative and quantitative information about the FN adsorption on the samples, FITC-labeled FN was pre-adsorbed from a solution of 40 μg/ml in PBS with pH 7.3 at 37°C for 30 min and further observed with laser scanning confocal fluorescent microscopy (LSCM; Leica, Germany) at fixed excitation mode. Before coating each sample was washed with distilled water for 10 min and dried in air. FN coated samples were fixed with 3% paraformaldehyde after rinsing twice with PBS, mounted in Mowiol (Sigma, 324590) and viewed by LSCM at magnification 40×.

2.3 Cell culture and cell adhesion assay

Human osteoblast-like MG-63 cell line (purchased from ATCC, USA) was used as a model system to examine the effects of surface coatings on osteoblast adhesion, spreading and overall morphology, as well as on FN matrix organization. Cells were maintained in Dulbecco′s modified Eagle medium (Gibco, 11960-044) supplemented with 10% fetal bovine serum (FBS), 1% penicillin/streptomycin, 2 mM, L-glutamine and 1 mM sodium pyruvate (Gibco, 11360-039), in a humidified atmosphere of 5% CO_2 in air. The culture medium was exchanged every second day. Upon reaching confluence, cells were detached with 0, 05% trypsin–EDTA (Gibco, 25200-072) inactivated with FBS after detachment (approx. 5 min), and then cells were recultured or used for the experiments.

For cell adhesion studies, metal samples (22 × 22 mm) from the three groups (AP–ND, AP and SS) were coated for 30 min at 37°C with non-labeled FN at low (1 μg/ml) and high (20 μg/ml) concentrations dissolved in PBS. After coating the samples were washed twice with PBS. To obtain serum-coated samples, the samples were covered with pure fetal bovine serum (FBS; Gibco) and further processed under identical conditions. One set of samples has been precoated with proteins and another one studied as plain.

To investigate the overall morphology and initial cell adhesion and spreading, 2×10^4 cells were seeded on each surface placed on 6 well tissue culture plates in 2.0 ml serum free medium. After 2 h of incubation, the living cells were stained with fluorescein diacetate (FDA), adding 10 μl/ml to each sample from a stock of 5 mg/ml in acetone. FDA is transported across cell membranes of the living cells and deacetylated to fluorescent analogue by nonspecific esterases allowing direct visualization by fluorescent microscopy. Representative pictures of the adhering cells were taken on a fluorescent microscope (Zeiss, Axiovert 40, Germany, magnification 20×) equipped with a digital camera. At least three representative pictures of each sample were made and morphological parameters such as the adhesion and mean spreading area of the cells were evaluated using automated image analysis software (analySIS v. 3.0, Soft Imaging System GmbH). Focal adhesions formed by MG-63 cells were visualized on samples fixed as described above using specific mouse monoclonal antibody (Sigma) against vinculin (1:800 dilution) in 1% bovine serum albumin (BSA) followed by goat anti-mouse Cy3 conjugated secondary antibody (Jackson ImmunoResearch). The samples were mounted and viewed on inverted fluorescent microscope Axiovert as written above and at least three representative images were obtained.

2.4 Reorganization of adsorbed fibronectin (early FN matrix)

The ability of MG-63 cells to reorganize adsorbed FN (i.e. early matrix formation) was monitored on samples coated with FITC-labeled FN as already described before seeding with 2×10^4 cells/well in serum containing medium. After 5 h of incubation the samples were fixed using 3% paraformaldehyde, mounted in Mowiol, observed and photographed with a fluorescent microscope Axiovert. Regular round-shaped glass coverslips (Menzel GmbH & Co KG, D 15 mm) coated with FITC-FN where used as a positive control.

2.5 Fibronectin matrix formation (late FN matrix)

The ability of MG-63 cells to secrete and deposit FN into the ECM fibrils (i.e. late FN matrix formation) was examined via immunofluorescence for FN. For that purpose, 3×10^4 cells/well were cultured on the different samples for 3 days in 10% serum containing medium. At the end, the samples were rinsed with PBS, fixed with 3% paraformaldehyde for 5 min, washed and saturated with 1% BSA for 15 min. Subsequently samples were stained with a polyclonal rabbit anti-FN antibody (Sigma) dissolved in 1% albumin in PBS for 30 min, followed by goat anti-rabbit Alexa Fluor 555-conjugated secondary antibody (Invitrogen) for 30 min before washed, mounted with Mowiol, viewed and photographed on fluorescent microscope Axiovert.

2.6 Statistical analysis

Statistical analysis was performed using StatGraphics Plus software employing ANOVA test to determine statistically

significant differences between groups ($P < 0.05$). Each data point represents mean ± standard deviation (SD) from at least three independent experiments.

3 Results

3.1 Characterization of the AP–ND composite coating

As a result of the ED from the ND-containing SBF electrolyte, white, dense and homogeneous AP–ND composite coatings with needle-like morphology were deposited on the SS substrates as observed by SEM (Fig. 1a). In addition, white aggregates of needlelike crystals were found, randomly distributed along the underlying homogeneous coatings. The deposits on the AP control samples had the same morphology. Figure 1b shows the FTIR spectrum of the AP–ND coating. Highly intensive envelope of peaks due to $v_{2,4}$ PO_4^{3-} stretching modes was detected in the frequency region of 400–700 cm^{-1}. A broad peak envelope with lower intensity was observed at of 950–1180 cm^{-1}. Peak fitting revealed that it was an envelope of underlying peaks due to $v_{1,3}$ PO_4^{3-} stretching, v_2 CO_3^{2-} stretching and HPO_4^{2-} vibrational modes. In addition, two absorption peaks due to v_3 CO_3^{2-} stretching at 1430 and 1620 cm^{-1}, characteristic of partial CO_3 substitution of PO_4 ions in the AP structure was detected. Spectrum intensity of the AP–ND coating was lower than those of the AP coating (spectrum not shown since it was identical). Data for the Ca:P ratio of the AP–ND and AP coatings, obtained by EDX spectroscopy revealed higher value for the latter (1.40) in comparison to the composite coating (1.29). Thickness and calculated mechanical parameters—shear (τ) and peel (P) strengths, related to the coatings cohesion and coating-substrate adhesion, respectively, were obtained by SAICAS measurement system (Table 1). Both τ and P strengths increased as the ND particles were incorporated in the AP coatings (see data for the AP–ND samples).

Table 1 Calculated from SAICAS data for shear (τ) and peel (P) strengths (mean ± SD)

Sample	Shear strength (MPa)	Peel strength P (N/m)	Coating thickness d (nm)
AP	20.3 ± 0.4	33.5 ± 0.5	1033 ± 76
AP–ND	44.4 ± 11.1	51.0 ± 4.0	935 ± 240

Thickness of the AP–ND and AP coatings was estimated to be about 1 μm [31] by SAICAS. According to the HV results, the composite coating had higher HV value than the AP coating (HV 453.8 ± 66.7 vs. HV 373.7 ± 32.3). The same tendency was observed not only for the load of 245 mN but also at applying loads of 98, 490 or 980 mN. After testing the HV of the AP–ND coating, SEM images were taken again and they revealed that cracks extending from the corners of the imprint left by the diamond blade were absent [31]. No delamination of the coatings was observed even at testing with the highest load (980 mN).

3.2 Biological studies

To characterize the biocompatibility of AP–ND coating, initial adhesion of MG-63 cells on plain and serum-coated samples after 2 h of incubation was studied and compared to SS and single AP coating. The overall cell morphology on plain samples is shown on Fig. 2a–c. Although the cells attached slightly better on AP–ND they did not spread sufficiently on all non-coated samples, thus representing rounded morphology. Indeed, the quantitative data for cell adhesion (see Table 2a) showed a non-significant increase (about 20%) of cell number on AP–ND ($P > 0.05$) versus AP samples, while adhesion did not differ between plain AP–ND and SS samples. Coating of samples with serum significantly improved cellular interaction (Fig. 2d–f), pronouncedly on AP–ND surface (Fig. 2d), where both cell adhesion (Table 2a) and cell spreading area (Table 3a) increased significantly in comparison to the plain samples.

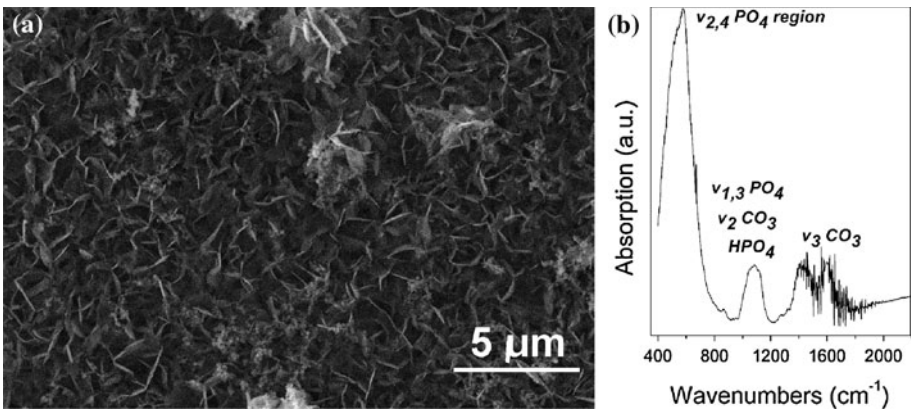

Fig. 1 **a** SEM reveals the formation of dense and homogeneous, non-stoichiometric AP–ND coating; **b** the coating is identified by FTIR as CO_3- and HPO_4-containing AP

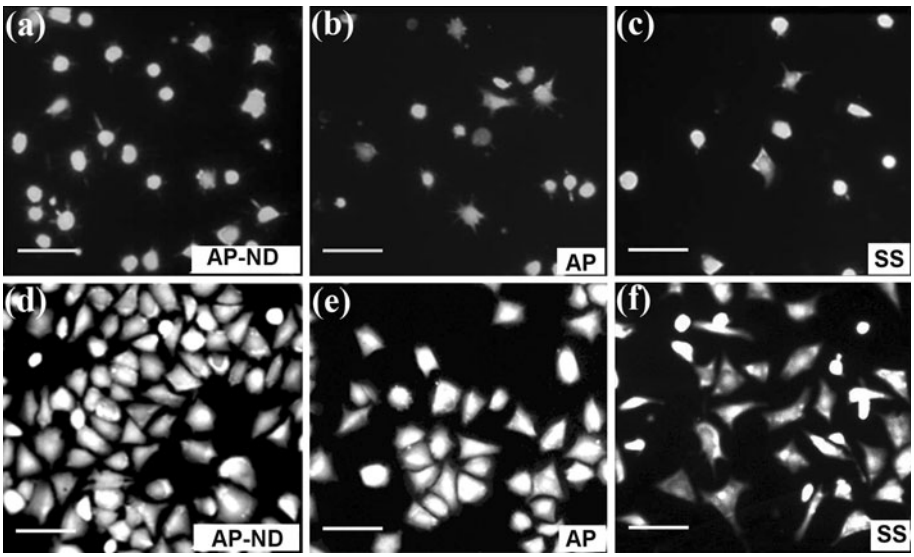

Fig. 2 Overall morphology of MG-63 cells adhering for 2 h on plain (**a–c**) and serum-coated AP–ND, AP or SS (**d–f**) samples (FDA staining; images taken on inverted fluorescent microscope, *bar* 100 μm)

Table 2 Adhesion of MG-63 cells to AP–ND, AP and SS samples after 2 h of cultivation in serum-free medium

Cell number (mm^2)		
Sample	FBS	Plain
(a)		
AP	207.5 ± 22.9	57.5 ± 10.1
AP–ND	257.0 ± 7.3*	69.3 ± 10.9
Stainless steel	133.2 ± 28.5	70.25 ± 18.7
Sample	FN 1 μg/ml	FN 20 μg/ml
(b)		
AP	134.5 ± 10.6	183.5 ± 17.3
AP–ND	171.5 ± 6.3*	200.3 ± 14.2
Stainless steel	85.66 ± 19.5	75.25 ± 21.9

Significantly different values are marked with *asterisk*

Within the group of serum coated samples, adhesion significantly increased on AP–ND coating ($P < 0.05$, Table 2a). Again a tendency for improved cell spreading on AP–ND samples was observed, however it was not statistically significant ($P > 0.05$, Table 3a).

FN is a main adhesive protein in blood although persisting in low amounts in the commercial serum preparations [32]. Therefore, we followed its adsorption profile in a single protein system. FN was labeled with FITC and adsorbed from a concentration of 20 μg/ml then viewed on LSCM using the z-stacks mode to overcome the impact of surface roughness. To compare FN adsorption between different samples we used fixed excitation intensity mode. As seen in Fig. 3, we found significantly increased intensity of the adsorbed FITC-FN to AP–ND surface versus pure AP samples (the SS samples were not studied because of their highly reflective surface). Quantitative analysis of the fluorescent intensity in grayscale pixels (values were obtained from five different LSCM images) at different points of the samples revealed statistically significant increase ($P < 0.05$) in adsorption of FITC-FN to AP–ND (191.1 ± 1.6) in comparison to pure AP (74.0 ± 4.3).

Further, MG-63 cells were used to screen the biological activity of adsorbed FN. Assuming that FN amount was relatively low in the commercial serum preparations (FN binds to fibrin during blood clotting) it was adsorbed at low (1 μg/ml), and at relatively high (20 μg/ml) concentrations (e.g. below and above the saturation, respectively). Figure 4 reveals that FN significantly improved the cellular interaction to all samples (see Fig. 2a–c), but it depended on the coating concentration. Substantially increased adhesion of MG-63 cells was found on AP–ND at low FN adsorption concentration (Fig. 4a), compared to AP (Fig. 4b) and SS (Fig. 4c), and this tendency was confirmed from the quantitative measurement of cell adhesion (Table 2b) where statistically significant increase of adhesion to AP–ND (171.5 ± 6.3 cells/mm^2 vs. 134.5 ± 10.6 on AP and 85.66 ± 85.66 on SS) was evaluated. Increase

Table 3 Spreading of MG-63 cells on AP–ND, AP and SS samples after 2 h of incubation in serum-free medium

Cell spreading area (μm^{-2})		
Sample	FBS	Plain
(a)		
AP	1284 ± 393	715 ± 312
AP–ND	1414 ± 521	800 ± 315
Stainless steel	1142 ± 602	673 ± 375
Sample	FN 1 μg/ml	FN 20 μg/ml
(b)		
AP	1431 ± 603	1836 ± 718
AP–ND	1533 ± 697	1963 ± 759
Stainless steel	1276 ± 582	1682 ± 458

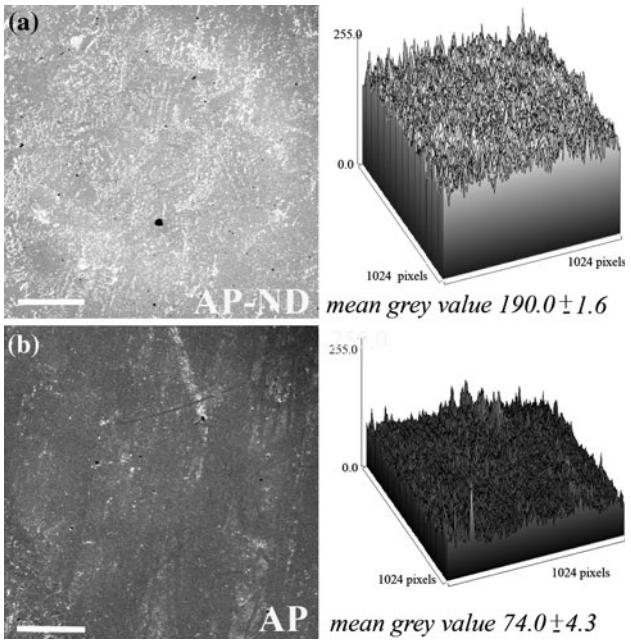

Fig. 3 2D and 3D confocal images of adsorbed FITC-FN on AP–ND (**a**) and pure AP (**b**) coatings (images taken on LSCM, *bar* 50 μm)

of cell spreading on AP–ND was also observed (Table 3b) but it was not statistically significant. Conversely, the saturating concentrations of FN (20 μg/ml) abolished the difference between samples.

The formation of focal adhesion complexes is another sign for the effectiveness of cell–substratum interaction. The focal contacts are the sites where the real physical adhesion to the material takes place [33] and to visualize them we used immunofluorescence for vinculin. As shown in Fig. 5e and f no significant formation of focal contacts was found on the plain AP and AP–ND surfaces although more cells attached on AP–ND. Conversely, on both serum and FN-coated samples (Fig. 5a–d) cells acquired flattened morphology (as on Fig. 2d–f) corroborating well with the development of focal adhesion complexes, better expressed on AP–ND samples.

It is well documented that many types of cells not only attach to adsorbed FN but also tend to rearrange it in a fibril-like pattern, presumably as an attempt to organize their own early matrix [34–36]. As some surfaces can promote FN reorganization [35], we followed this process using MG-63 cells as a model system. For that purpose we cultured the cells for 5 h on FITC-FN coated samples and on hydrophilic glass slides as positive controls. As seen in Fig. 6a, cells on AP–ND surface rearranged well the adsorbed FN in almost undistinguishable pattern from the control. FITC-FN appeared as bright streaks on the dark background of removed FN, which otherwise was well visible on the rest of substratum thus forming linear matrix-like structure above or beneath the cells. When fluorescent and phase contrast images were merged, more than 90% of the reorganized FN was associated with osteoblasts (data not shown) in accordance with our previous studies [34–36]. In contrast, only small patches of FN rearrangement were found on pure AP coating and plain SS surfaces (Fig. 6b and d, respectively), indicating reduced matrix-forming activity.

At longer incubations osteoblasts produce osseogenic matrix [8] containing various matrix components, including FN [17]. To learn whether the initial difference in FN adsorption will affect the development of osteoblast FN matrix, we cultured MG-63 cells for 3 days before FN was visualized via immunofluorescence. Multiple bright fibrils forming typical networks were observed on all samples (Fig. 7), however they were the strongest on the AP–ND samples (Fig. 7a) suggesting promoted FN matrix formation in comparison to the plain AP (Fig. 7b) and SS (Fig. 7c).

4 Discussion

SEM imaging revealed that the composites deposited on the SS substrates for 15, 30 or 60 min in the ND-containing SBF electrolyte were white, dense and homogeneous

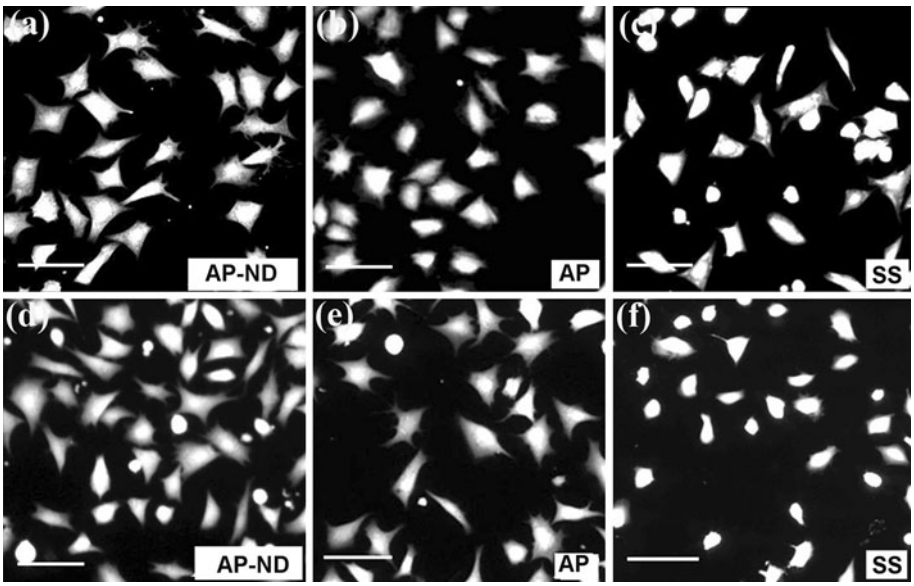

Fig. 4 Overall morphology of MG-63 cells adhering for 2 h on AP–ND, AP or SS samples coated with high (20 μg/ml; **a**–**c**) or low FN concentration (1 μg/ml; **d**–**f**) (FDA staining; images taken on inverted fluorescent microscope, *bar* 100 μm)

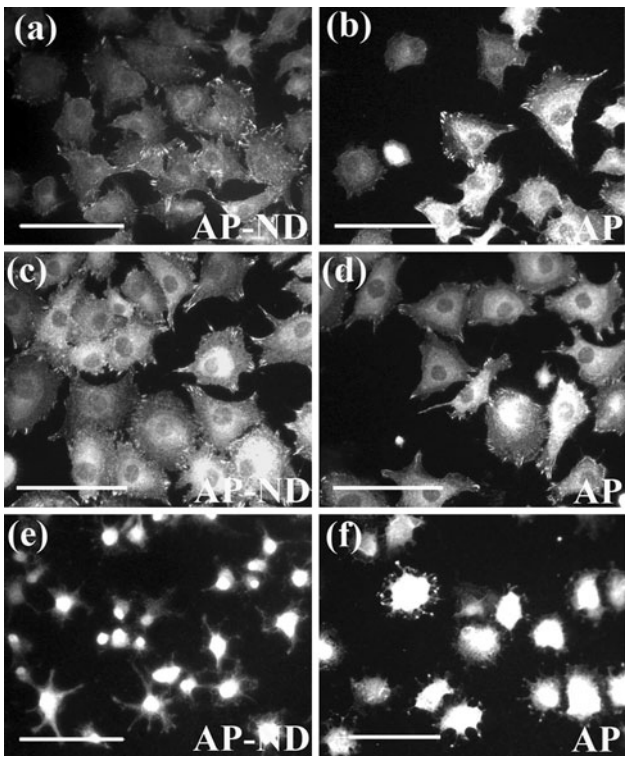

Fig. 5 Overall morphology and focal adhesion formation of MG-63 cells adhering for 2 h on AP–ND (**a**, **c**, **e**) and pure AP (**b**, **d**, **f**). Samples are coated with serum (**a**, **b**), with FN (**c**, **d**) or studied as plain (**e**, **f**) (vinculin staining; images taken on inverted fluorescent microscope, *bar* 100 μm)

coatings with needle-like morphology and randomly distributed white aggregates of needlelike crystals (Fig. 1a). Electrodeposition of the control AP coatings did not yield different morphology, which means that the method utilized for the coating of the SS substrates from ND-containing or pure SBF electrolyte was not decisive for the coating morphology. Based on the observation that broad peaks characteristic of PO_4^{3-}, CO_3^{2-} and HPO_4^{2-} vibrational modes were found in the FTIR spectra of both AP–ND and AP coatings, it was concluded that nonstoichiometric, CO_3^{-} and HPO_4^{-} containing AP was grown. The FTIR data also revealed CO_3 substitution of PO_4 ions in the AP structure. The lower spectrum intensity measured for the AP–ND coatings in comparison to the control AP was attributed to lower thickness (as known, peak intensity is proportional to the coating thickness according to the Beer's Law [37]); probably the AP growth was retarded with the incorporation of the ND particles [31]. It is known that the Ca:P value of a stoichiometric HA is 1.67 [28]. The lower Ca:P values for both composite and control coatings obtained in this work could be attributed either to lower crystallinity AP or to a combination of crystalline HA and other calcium phosphate phases, which also contribute to a decrease of the coating crystallinity and Ca:P ratio [28]. The lower Ca:P value of the AP–ND coatings could be also attributed to some degree of amorphisation, which the ND particles introduced in the non-stoichiometric coatings as discussed for the FTIR data [31]. The increase of τ and P strengths after the incorporation of the ND particles in the AP coating (see data in Table 1 for the AP–ND samples) revealed enhanced cohesion of the composite coatings and their adhesion to the SS substrates, probably due to the presence of the ND particles as a second minor phase.

High hardness is a guarantee for a good wear resistance, which is crucial for the AP implant coatings. Although the low initial concentration of the ND particles in the ND-containing SBF electrolyte (0.5 g/l) and the sedimentation of the bigger particles with the ED time, the AP hardness was improved with the addition of the ND

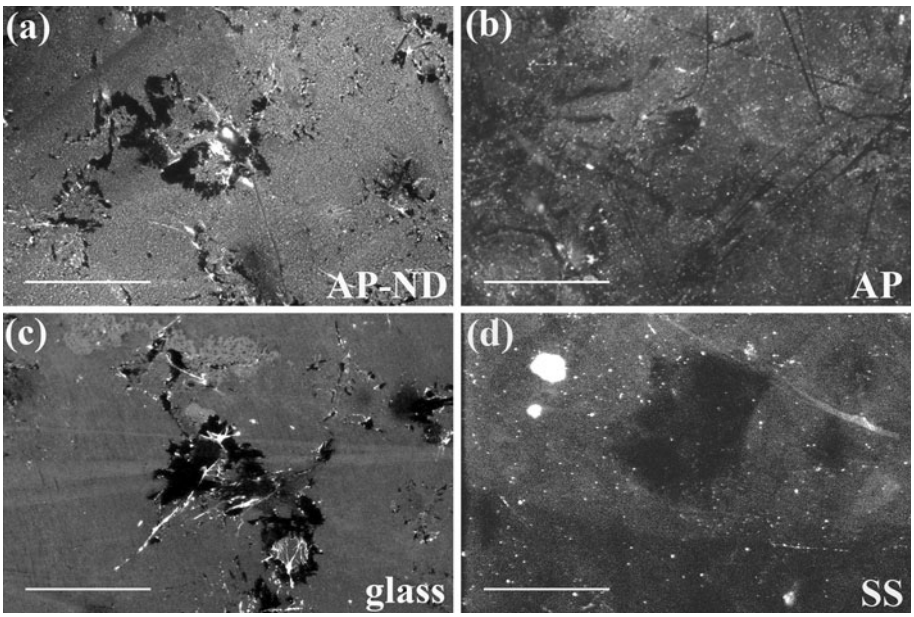

Fig. 6 Early FN matrix formation on AP–ND (**a**) and AP (**b**) coatings compared with control glass (**c**) and SS (**d**) surfaces (images taken on inverted fluorescent microscope, *bar* 100 μm)

particles as seen by the HV results—HV of the AP–ND and AP coatings was 453.8 and 373.7 respectively [31]. The lack of cracks extending from the corners of the imprint left by the diamond blade [31] testified for the good ductility and the lack of residual stress of the composites.

The biological results presented here illustrate the significant role of FN for the in vitro response of osteoblast like cells to this new HA biomaterial. Biomimetic HA is a highly biocompatible inorganic material from the apatite (AP) family and it osseointegrates well due to its chemical resemblance to mammalian bone and teeth [4, 5, 27], therefore metal implants are frequently coated with HA in order to facilitate bone adaptation, firmer implant-bone attachment, which leads to a reduced healing time and enhanced bone apposition in comparison to uncoated implants [4, 5]. However, the molecular mechanism standing behind this facilitated osseointegration remains unclear, and usually is attributed to the mechanical resemblance with surrounding tissues. We anticipate that it is due to the strong ability of HA to adsorb ECM proteins, which lead to improved cellular interaction and also matrix deposition. As osteoblastls are the principal cells in the bone matrix their successful interaction with a material provides insights on its osseointegration [27]. Osteoblasts express a variety of integrins that bind with high affinity to ECM proteins such as fibronectin, osteonectin and different collagens [11]. Therefore, their interaction with given material should be explored in the context of distinct proteins recognition. It is well documented that implanted materials are immediately covered with proteins from the blood or interstitial fluids. Hence, it is the adsorbed proteins, rather than the surface itself which cells really "sense" and interact with [38]. Indeed, our studies show that the coating of samples with serum significantly improved cellular interaction, pronouncedly on AP–ND coating, which raise the question which proteins are involved. In this respect the particular impact of FN is very important as it is the main adhesive protein in the biological fluids. However it persists in a very low amount in the commercial serum preparations [32] as it binds to fibrin during the clot formation. Therefore, to follow it adsorption profile we used a single protein system. Indeed, the significant increase of adsorbed FITC-FN to AP–ND surface versus pure AP suggest it particular impact in the osteoblast interaction. We hypothesized that the increased amount of adsorbed FN may be due to the presence of NDs. The literature shows that this truly nanoscale material possess extremely high surface area, surface charge and express various active functional groups such as OH^{-}, $COOH^{-}$, NH^{2+} or SO_3H^{-}, as a result of the detonation process [39, 40]. NDs are considered for biomedical application due to their high adsorption capacity, caused by the increased specific surface area, but also because of demonstrated chemical inertness in contact with biological entities [41]. It is clear however that not only the adsorption of biological molecules but also their conformation will influence the consequent cellular interaction. There are four different morphological patterns of adsorbed FN found on HA-based coatings: (i) homogeneous, (ii) as aggregates, (iii) as isolated fibrils, or (iv) as interconnected fibrils [16]. Indeed, our representative images in Fig. 3 showed that the adsorption of FN on both AP and AP–ND coatings was rather heterogeneous, with appearing of dot-like pattern of aggregates that often arranged in a striate structures, presumably following the spontaneous organization of the AP crystals. As these linear features were pronouncedly

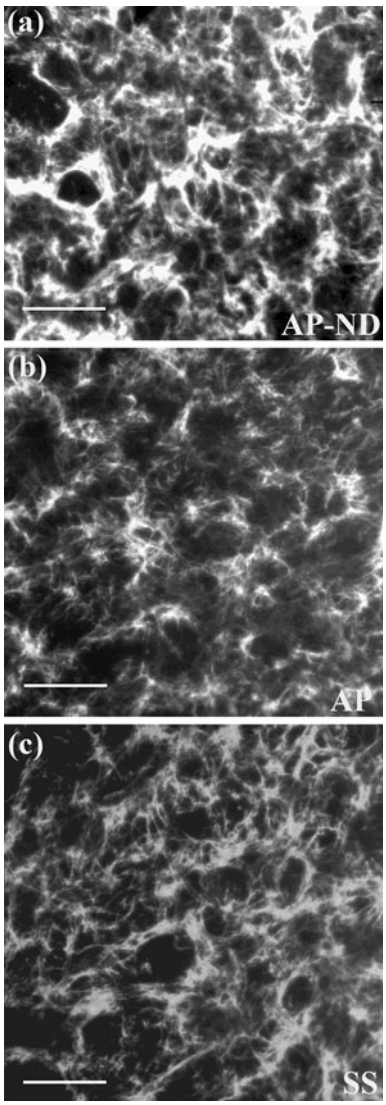

Fig. 7 Late FN matrix deposition on AP–ND (**a**), AP (**b**) and SS (**c**) samples (immunofluorescence for FN is observed on inverted fluorescent microscope, *bar* 100 μm)

expressed on AP–ND samples, we anticipate that the spontaneous formation of such oriented structures could also promote interaction with cells [11, 16, 22]. Although no FN fibrils formation was observed it does not necessarily mean an absence of small micro/nanofibrils, as the characteristic scale could lie below the optical resolution. Out of these arrangements, FN showed homogenous adsorption pattern.

Several studies have demonstrated that cell adhesion and spreading is highly dependent on the conformation of adsorbed proteins. Indeed, the present study shows that AP–ND triggers specific interaction with the protein molecules and as FN fibril formation is dependent on its solution concentration [42] we assume that the cellular interaction is also concentration dependent. Thus, following our finding we anticipate that the effect of serum on the AP–ND coating is caused by the greater affinity for FN which compensates its lowered amount [32]. Another measure for the effectiveness of cell—substratum interaction is the formation of focal adhesion complexes which determine the successful transmission of signals to the cell interior through integrin based mechanism [43]. Although we did not study the distribution of integrin receptors involved in FN recognition, we found the same correlations between the focal adhesions formation and the improved osteoblast interaction on both serum and FN coated AP–ND samples, again suggesting that it results from the higher affinity for FN.

Our previous studies suggests that materials need to adsorb matrix proteins loosely in order to be biocompatible [34–36]. In this respect the present results show that osteoblasts tend to reorganize adsorbed FN much better on AP–ND surface, which leads to the assumption that FN is rather loosely bound, e.g. in such a way that the cells could easily remove and organize it in a matrix-like structure [34–36], apart from pure AP and SS substrates. One can support that the reduced reorganization activity on pure AP and SS materials might be relative, caused from the less FN adsorption. However on the better biocompatibility of the hybrid AP–ND coating again point the results for the "late" matrix formation demonstrating much stronger deposition of FN matrix fibrils on these samples.

5 Conclusions

This study shows that AP–ND coating significantly enhance FN adsorption in comparison to pure AP and SS substrata in the same time promoting osteoblasts attachment and the organization of provisional FN matrix. The overall cell morphology, the quantities for cell adhesion and spreading and the better focal adhesions formation reveal promoted cellular interaction presumably caused by the greater FN adsorption. Collectively, these data imply on the improved biocompatibility of the composite AP–ND coating in osseogenic environment.

Acknowledgments The authors acknowledge the support of grants TK-X-1708/2007 of the National Science Fund of the Bulgarian Ministry of Education and Science (to LP and EP), EUREKA project E13033 BIONANOCOMPOSIT (to LP and EP), NATO grant CBP.EAP.RIG.982693 (to EP), and grant MAT2006-11516 provided from the Spanish Ministry for Education and Science (to GA).

References

1. Schliephake H, Scharnweber D, Dard M, Rössler S, Sewing A, Hüttmann C. Biological performance of biomimetic calcium phosphate coating of titanium implants in the dog mandible. J Biomed Mater Res. 2002;64 A(2):225–34.

2. Catledge S, Fries M, Vohra Y, Lacefield W, Lemons J, Woodard S, Venugopalan R. Nanostructured ceramics for biomedical implants. J Nanosci Nanotechnol. 2002;2:293–312.
3. LeGeros R. Properties of osteoconductive biomaterials: calcium phosphates. Clin Orthop Relat Res. 2002;395:81–98.
4. Kilpadi K, Chang P-L, Bellis S. Hydroxylapatite binds more serum proteins, purified integrins, and osteoblast precursor cells than titanium or steel. J Biomed Mater Res A. 2001;57:258–67.
5. Xie J, Baumann M, McCabe L. Osteoblasts respond to hydroxyapatite surfaces with immediate changes in gene expression. J Biomed Mater Res A. 2004;71:108–17.
6. Narayan R. Nanostructured diamondlike carbon thin films for medical applications. Mater Sci Eng C. 2005;25:405–16.
7. Catledge Sh, Fries M, Vohra Y. In: Nalwa H, editor. Encyclopedia of nanoscience and nanotechnology, vol. 10. American Scientific Publishers; 2004, p. 1.
8. Barrias C, Cristina M, Martins L, Almeida-Porada G, Barbosa M, Granja P. The correlation between the adsorption of adhesive proteins and cell behaviour on hydroxyl-methyl mixed self-assembled monolayers. Biomaterials. 2009;30:307–16.
9. Pankov R, Yamada KM. Fibronectin at a glance. J Cell Sci. 2002;115(Pt 20):3861–3.
10. Alves C, Yang Y, Carnes D, Ong J, Sylvia V, Dean D, Agrawal C, Reis R. Modulating bone cells response onto starch-based biomaterials by surface plasma treatment and protein adsorption. Biomaterials. 2007;28:307–15.
11. Anselme K. Osteoblast adhesion on biomaterials. Biomaterials. 2000;21:667–81.
12. Wilson C, Clegg R, Leavesley D, Pearcy M. Mediation of biomaterial–cell interactions by adsorbed proteins: a review. Tissue Eng. 2005;11(1–2):1–18.
13. Akiyoshi K, Yasuaki T, Akihiro O, Taichi N, Kazushi T, Junnosuke R. Effects of fibronectin on osteoinductive capability of fresh iliac bone marrow aspirate in posterolateral spinal fusion in rabbits. Spine. 2008;33(12):1318–23.
14. Vogel V, Baneyx G. The tissue engineering puzzle: a molecular perspective. Ann Rev Biomed Eng. 2003;5:441–63.
15. Woo K, Seo J, Zhang R, Ma P. Suppression of apoptosis by enhanced protein adsorption on polymer/hydroxyapatite composite scaffolds. Biomaterials. 2007;28(16):2622–30.
16. Lebaron RG, Athanasiou KA. Extracellular matrix cell adhesion peptides: functional applications in orthopedic materials. Tissue Eng. 2000;6(2):85–103.
17. Velling T, Risteli J, Wennerberg K, Mosher D, Johansson S. Polymerization of type I and III collagens is dependent on fibronectin and enhanced by integrins $\alpha_{11}\beta_1$ and $\alpha_2\beta_1$. J Biol Chem. 2002;277:37377–81.
18. Pereira M, Rybarczyk B, Odrljin T, Hocking D, Sottile J, Simpson-Haidaris P. The incorporation of fibrinogen into extracellular matrix is dependent on active assembly of a fibronectin matrix. J Cell Sci. 2002;115:609–17.
19. Sottile J, Hocking D. Fibronectin polymerization regulates the composition and stability of extracellular matrix fibrils and cell-matrix adhesions. Mol Biol Cell. 2002;13:3546–59.
20. Dallas S, Sivakumar P, Jones C, Chen Q, Peters D, Mosher D. Fibronectin regulates latent transforming growth factor-β (TGFβ) by controlling matrix assembly of latent TGFβ-binding protein-1. J Biol Chem. 2005;280:18871–80.
21. Garcia AJ. Get a grip: integrins in cell–biomaterial interactions. Biomaterials. 2005;26:7525–9.
22. Reyes C, Petrie T, García A. Mixed extracellular matrix ligands synergistically modulate integrin adhesion and signaling. J Cell Physiol. 2008;217:450–8.
23. Plow EF, ThA Haas, Zhang L, Loftus J, Smith JW. Ligand binding to integrins. J Biol Chem. 2000;275:21785–8.
24. Akiyama SK. Integrins in cell adhesion and signaling. Hum Cell. 1996;9(3):181–6.
25. Vial D, Monaghan-Benson E, McKeown-Longo P. Coordinate regulation of fibronectin matrix assembly by the plasminogen activator system and vitronectin in human osteosarcoma cells. Cancer Cell Int. 2006;6:8.
26. Daley W, Peters S, Larsen M. Extracellular matrix dynamics in development and regenerative medicine. J Cell Sci. 2008;121:255–64.
27. Baxter L, Frauchiger V, Textor M, Gwynn Iap, Richards R. Fibroblast and osteoblast adhesion and morphology on calcium phosphate surfaces. Eur Cells Mater. 2002;4:1–17.
28. Pramatarova L, Pecheva E. Materials science foundations, vol. 26. Uetikon-Zurich: Trans Tech Publications; 2006.
29. Kokubo T, Takadama H. How useful is SBF in predicting in vivo bone bioactivity? Biomaterials. 2006;27:2907–15.
30. Stavrev S, Lazarov S, Stoev Kh, Markov L, Ivanov V. Method for production of ultra-dispersed diamond. US patent 5353708; 1994.
31. Pecheva E, Pramatarova L, Hikov T, Fingarova D, Tanaka Y, Sakamoto H, Doi H, Tsutsumi Y, Hanawa T. Apatite–nanodiamond composite as a functional coating of stainless steel. Surf Interf Anal. 2010;42:475–80.
32. Hynes RO. Fibronectins. New York: Springer-Verlag; 1990.
33. Campbell ID. Studies of focal adhesion assembly. Biochem Soc Trans. 2008;36:263–6.
34. Altankov G, Groth Th. Fibronectin matrix formation by human fibroblasts on surfaces varying in wettability. J Biomater Sci Polym Ed. 1997;8:299–310.
35. Groth Th, Altankov G. In: Ottenbrite RM, Sunamoto I, editors. Frontiers in biomedical polymer applications. Lancaster-Basel: Technomics Publisher Inc.; 1998.
36. Groth Th, Altankov G. In: Harris P, Chapman D, editors. New biomedical materials. IOS Press; 1998.
37. Socrates L. Infrared characteristic group frequencies. New York: Wiley; 1980.
38. Wilson CJ, Clegg RE, Leavesley DI, Pearcy MJ. Mediation of biomaterial–cell interactions by adsorbed proteins: a review. Tissue Eng. 2005;11(1–2):1–18.
39. Mykhaylyk O, Solonin Y, Batchelder D, Brydson R. Transformation of nanodiamond into carbon onions: a comparative study by high-resolution transmission electron microscopy, electron energy-loss spectroscopy, X-ray diffraction, small-angle X-ray scattering, and ultraviolet Raman spectroscopy. J Appl Phys. 2005;97:074302. doi:10.1063/1.1868054.
40. Baidakova M, Vul A. New prospects and frontiers of nanodiamond clusters. J Phys D: Appl Phys. doi:10.1088/0022-3727/40/20/S14.
41. Khabashesku V, Margrave J, Barrera E. Functionalized carbon nanotubes and nanodiamonds for engineering and biomedical applications. Diamond Relat Mater. 2005;14:859–66.
42. Salmerón-Sánchez M, Rico P, Moratal D, Lee TT, Schwarzbauer JE, García AJ. Role of material-driven fibronectin fibrillogenesis in cell differentiation. Biomaterials. 2011;32:2099–105.
43. Bush KA, Driscoll PF, Soto ER, Lambert CR, McGimpsey WG, Pins GD. Designing tailored biomaterial surfaces to direct keratinocyte morphology, attachment, and differentiation. J Biomed Mater Res A. 2009;90(4):999–1009.